

The $B^2\Pi-X^2\Pi$ electronic origin band of $^{13}\text{C}_6\text{H}$

X. Bacalla^{a,b}, D. Zhao^b, E.J. Salumbides^{a,c}, M.A. Haddad^{a,1}, H. Linnartz^b, W. Ubachs^{a,*}

^aDepartment of Physics and Astronomy, LaserLaB, VU University, De Boelelaan 1081, 1081 HV Amsterdam, The Netherlands

^bSackler Laboratory for Astrophysics, Leiden University, Leiden Observatory, PO Box 9513, 2300 RA Leiden, The Netherlands

^cDepartment of Physics, University of San Carlos, Cebu City 6000, Philippines

Abstract

The rotationally resolved spectrum of the $B^2\Pi-X^2\Pi$ electronic origin band transition of $^{13}\text{C}_6\text{H}$ is presented. The spectrum is recorded using cavity ring-down spectroscopy in combination with supersonic plasma jets by discharging a $^{13}\text{C}_2\text{H}_2/\text{He}/\text{Ar}$ gas mixture. A detailed analysis of more than a hundred fully-resolved transitions allows an accurate determination of the spectroscopic parameters for both the ground and electronically excited state of $^{13}\text{C}_6\text{H}$.

Keywords: hexatriynyl radical, cavity ring-down spectroscopy, isotopic substitution, supersonic plasma discharge

1. Introduction

The hexatriynyl radical C_6H , a member of the linear C_{2n}H series, belongs to the spectroscopically best studied carbon chain radicals. The $X^2\Pi$ ground state was studied extensively in Fourier-transform microwave (MW) studies, yielding accurate constants [1–3]. The laboratory data followed astronomical detections of this molecule in the cold dense cloud TMC-1 [4, 5]. Later this molecule was detected along other lines of sight as well, e.g. towards the carbon rich star IRC+10216 [6]. The $B^2\Pi-X^2\Pi$ electronic spectrum of C_6H was reported in several studies. The first data were recorded in Ne matrix isolation studies after mass selective deposition [see e.g. 7]. This provided approximate values for the gas phase absorptions. The first gas phase spectrum was obtained under somewhat poor experimental conditions, using a hollow cathode discharge cell [8]. The resulting spectrum only showed unresolved features, including many bands starting from vibrationally excited states. Subsequently, high precision and rotationally resolved spectra were recorded using a new planar plasma source design [9] that allowed the detection of rotationally cold C_6H and C_6D transients under nearly Doppler-free conditions [2]. Combined with sensitive detection techniques, such as cavity ring-down spectroscopy, it was possible to realize excellent S/N ratios, not only for the origin band but also for transitions involving vibrationally excited levels in the upper electronic state. In combination with the available MW constants it was possible to derive precise upper state constants, for both spin-orbit components. Recently, a substantially extended study of these electronic bands, as well as new transitions involving vibronic hot bands was presented, with a focus on Renner-Teller effects in C_6H [10]. In the present work we extend previous spectroscopic

studies to the fully ^{13}C -substituted isotopologue $^{13}\text{C}_6\text{H}$. The rotationally resolved electronic spectrum yields accurate spectroscopic constants, also including the ground state constants that have not been determined before.

2. Experiment/method

We follow an established method that has been used successfully to record electronic spectra of many different carbon chain radicals before. Details of the experimental setup and experimental procedures are available from [9–11]. Supersonically jet-cooled $^{13}\text{C}_6\text{H}$ radicals are produced – among other species – in a pulsed (~ 10 Hz) planar or pinhole plasma expansion generated by discharging a high pressure (10 bar) gas pulse comprising of 0.18% ^{13}C -enriched (99% purity) C_2H_2 in a helium:argon $\sim 85:15$ mixture. Both slit and pinhole discharge nozzles, which have been used to study $^{12}\text{C}_6\text{H}$ in Ref. [10], are employed in the present experiment. The $3\text{ cm} \times 300\text{ }\mu\text{m}$ slit discharge nozzle, with typical discharge I/V values of $\sim 100\text{ mA}/\sim 750\text{ V}$ per jaw, is used to generate a planar plasma expansion with a nearly Doppler-free environment and a relatively long effective absorption path length. The pinhole nozzle system, with typical I/V $\sim 80\text{ mA}/\sim 1000\text{ V}$ values, generates a plasma expansion suffering from a somewhat larger Doppler width, but allows measuring spectra with different rotational temperatures in a more convenient way. Final rotational temperatures typically amount to 15–30 K.

The $^{13}\text{C}_6\text{H}$ spectra are recorded in direct absorption using cavity ring-down laser spectroscopy. Tunable light around 525 nm – the region where regular C_6H has been found – is generated using a Nd:YAG pumped pulsed dye laser (~ 6 ns pulse duration). The bandwidth of the dye laser is $\sim 0.035\text{ cm}^{-1}$, well below the expected line splitting between two adjacent rotational transitions. The light pulse is spatially filtered and enters a 58 cm long optical cavity comprising of two high reflection mirrors. The optical axis is aligned a few mm downstream, par-

* Corresponding author.

Email address: w.m.g.ubachs@vu.nl (W. Ubachs)

¹ Present address: Atomic and Molecular Group, Faculty of Physics, Yazd University, Yazd, Iran.

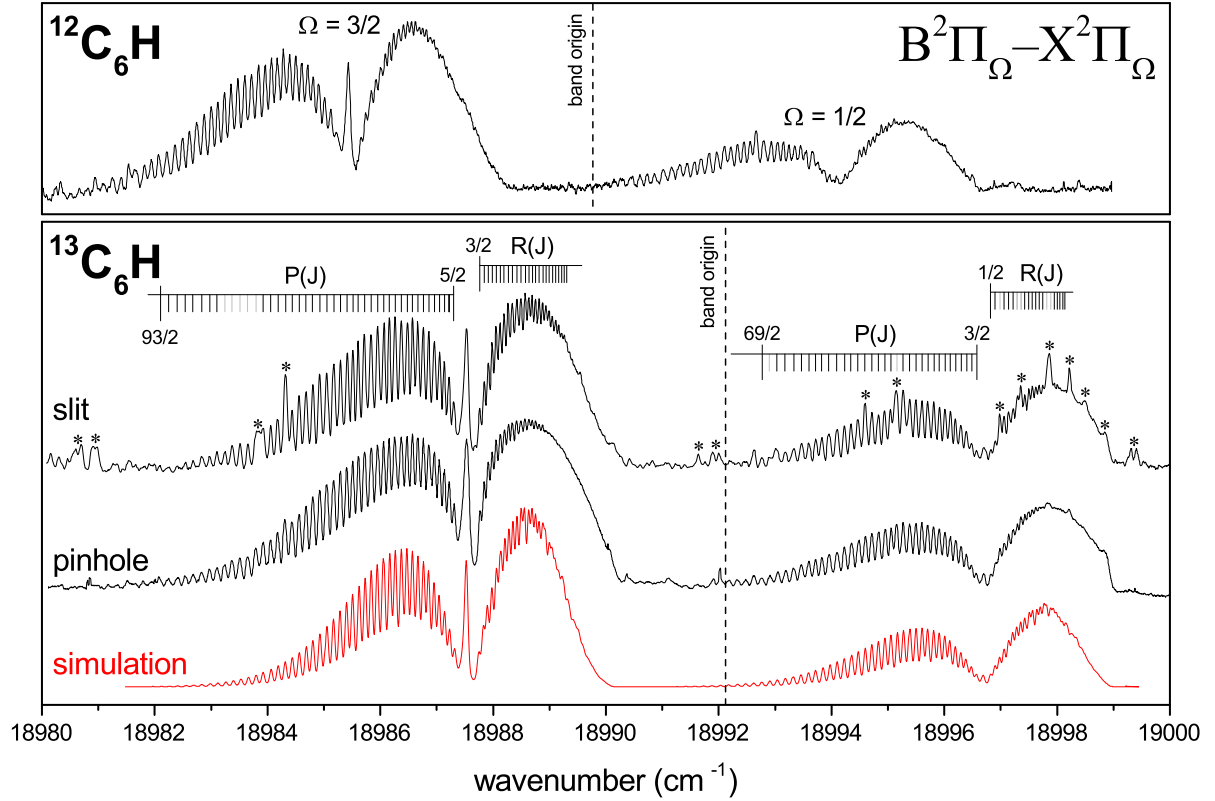


Figure 1: The $B^2\Pi-X^2\Pi$ electronic transition of $^{12}\text{C}_6\text{H}$ (upper panel) and $^{13}\text{C}_6\text{H}$ (lower panel) for a planar (slit) and a pinhole plasma expansion. Features indicated by an asterisk are due to other species and are mainly visible in the slit nozzle plasma. A simulated spectrum for $^{13}\text{C}_6\text{H}$ is shown in the lowest trace, based on the constants listed in Table 2 and a rotational temperature of $T_{\text{rot}} = 20.3(1)$ K.

allel to the slit or below the pinhole of the nozzle. Light leaking out of the cavity is recorded by a photo-multiplier tube and a spectrum is obtained by recording the ring-down time as function of the laser wavelength. Typical ring-down times amount to 40-100 μs . A precise pulse generator coordinates that the gas and the discharge pulse, and as well as the ring-down event, coincide. Simultaneously with the spectral recordings of $^{13}\text{C}_6\text{H}$, transmission fringes of an etalon (with a free spectral range of ~ 20.1 GHz) are recorded, providing relative frequency markers to correct for a possible non-linear wavelength scanning of the dye laser. An iodine spectrum allows an absolute wavelength calibration with an accuracy better than 0.02 cm^{-1} .

3. Results and analysis

In Figure 1 the $B^2\Pi-X^2\Pi$ electronic origin band (0_0^0) transition of regular C_6H (upper panel) and of $^{13}\text{C}_6\text{H}$ (lower panel) is shown. The newly recorded $^{12}\text{C}_6\text{H}$ spectrum compares well with data presented in [2, 10]. From a comparison of both panels it can be concluded that the ^{13}C -sample is highly pure, as nearly no features due to ^{12}C contamination can be clearly seen. Some extra lines in the lower panel – recorded through the slit expansion – are due to overlapping hot band transitions of other small hydrocarbons in the plasma. Previous work has shown that these lines become much weaker using the pinhole discharge nozzle, as visible from the corresponding spectrum. It should be noted that in contrast to the pinhole nozzle experiments in [10], the final Doppler width of individual transitions

is smaller, mainly because of the reduced expansion velocity of the jet that is run with more argon in the gas mixture.

The overall spectral pattern of $^{13}\text{C}_6\text{H}$ is very similar to that of $^{12}\text{C}_6\text{H}$, with a blue shift of $\sim 2 \text{ cm}^{-1}$. Both spectra consist of two components, each with (fully resolved) P, Q and (partially resolved) R branches, reflecting transitions between the two spin-orbit components: $B^2\Pi_{3/2}-X^2\Pi_{3/2}$ and $B^2\Pi_{1/2}-X^2\Pi_{1/2}$. The two band systems are split by $\Delta A = |A'-A''|$, the difference between the spin-orbit splitting in ground and excited state. An assignment of the individual spin-orbit components is straightforward; with a low final temperature in the jet expansion, the more intense component corresponds to a transition from the lower spin-orbit state, i.e. $X^2\Pi_{3/2}$ for C_6H . The observation of the barely visible Q-branch in the $B^2\Pi_{1/2}-X^2\Pi_{1/2}$ system provides further evidence for this assignment, as the intensity of the Q-branch scales quadratically with the value of the spin-orbit angular momenta (Ω^2).

The detailed rotational assignments for $^{13}\text{C}_6\text{H}$ are shown in Figure 1. The determined transition energies of the 116 assigned lines listed in Table 1 are used to fit five parameters. For regular C_6H a full analysis has been presented before [2, 10], guided by accurate ground state constants available from MW work [1, 2]. The focus here is on $^{13}\text{C}_6\text{H}$ for which ground state constants are not available; it is important, therefore, to realize that ground and excited state parameters may correlate in a fit.

The rotational analysis is performed using PGOPHER [12] software. The transition frequencies are fitted using a standard Hamiltonian for a $^2\Pi - ^2\Pi$ electronic transition, with the band

Table 1: The observed line positions (in cm^{-1}) for the two spin orbit components of the $\text{B}^2\Pi\text{--X}^2\Pi$ electronic transition of $^{13}\text{C}_6\text{H}$.

P-branch		$\text{B}^2\Pi_{3/2}\text{--X}^2\Pi_{3/2}$		$\text{B}^2\Pi_{1/2}\text{--X}^2\Pi_{1/2}$		R-branch		$\text{B}^2\Pi_{3/2}\text{--X}^2\Pi_{3/2}$		$\text{B}^2\Pi_{1/2}\text{--X}^2\Pi_{1/2}$	
J'	J''	Observed	o-c	Observed	o-c	J'	J''	Observed	o-c	Observed	o-c
0.5	1.5			18996.57	0.003	1.5	0.5			18996.82	-0.001
1.5	2.5	18987.30	-0.017	18996.48	0.003	2.5	1.5	18987.73	-0.007	18996.90	0.000
2.5	3.5	18987.22	-0.010	18996.39	0.003	3.5	2.5	18987.82	-0.007	18996.99	0.002
3.5	4.5	18987.14	-0.002	18996.29	0.001	4.5	3.5	18987.90	-0.001	18997.06	-0.001
4.5	5.5	18987.05	0.008	18996.20	-0.002	5.5	4.5	18987.98	0.003	18997.14	0.000
5.5	6.5	18986.96	0.006	18996.11	0.002	6.5	5.5	18988.06	0.004	18997.22	0.007
6.5	7.5	18986.86	-0.002	18996.02	0.008	7.5	6.5	18988.13	-0.001	18997.29	0.001
7.5	8.5	18986.76	-0.006	18995.92	0.007	8.5	7.5	18988.20	-0.005	18997.36	-0.003
8.5	9.5	18986.66	-0.004	18995.81	0.006	9.5	8.5	18988.27	-0.014	18997.43	-0.004
9.5	10.5	18986.57	0.002	18995.70	-0.010	10.5	9.5	18988.34	-0.013	18997.50	0.000
10.5	11.5	18986.48	0.012	18995.60	-0.003	11.5	10.5	18988.42	-0.003	18997.56	-0.006
11.5	12.5	18986.38	0.009	18995.51	0.009	12.5	11.5	18988.49	0.002	18997.63	-0.009
12.5	13.5	18986.26	-0.004	18995.40	0.004	13.5	12.5	18988.57	0.010	18997.68	-0.014
13.5	14.5	18986.16	0.000	18995.27	-0.012	14.5	13.5	18988.63	0.005	18997.74	-0.019
14.5	15.5	18986.06	0.008			15.5	14.5	18988.69	0.001		
15.5	16.5	18985.95	0.006	18995.05	-0.007	16.5	15.5	18988.75	-0.001		
16.5	17.5	18985.85	0.010	18994.95	0.006	17.5	16.5	18988.82	0.002	18997.95	0.015
17.5	18.5	18985.74	0.008	18994.83	-0.001	18.5	17.5	18988.88	0.002	18998.00	0.010
18.5	19.5	18985.63	0.004	18994.71	-0.005	19.5	18.5	18988.94	0.004	18998.04	-0.004
19.5	20.5	18985.51	0.004	18994.60	0.000	20.5	19.5	18989.00	0.004	18998.10	-0.002
20.5	21.5	18985.40	0.002	18994.49	0.010	21.5	20.5	18989.05	0.005	18998.15	-0.004
21.5	22.5	18985.28	-0.005	18994.37	0.013	22.5	21.5	18989.11	0.009		
22.5	23.5	18985.16	-0.005	18994.24	0.007	23.5	22.5	18989.16	0.005		
23.5	24.5	18985.05	-0.002	18994.10	-0.007	24.5	23.5	18989.21	0.003		
24.5	25.5	18984.93	-0.002	18993.98	-0.002	25.5	24.5	18989.26	0.001		
25.5	26.5	18984.81	0.000	18993.85	-0.004	26.5	25.5	18989.31	-0.004		
26.5	27.5	18984.69	-0.001	18993.73	0.003						
27.5	28.5	18984.56	-0.008	18993.59	-0.003						
28.5	29.5	18984.44	-0.004	18993.46	0.008						
29.5	30.5	18984.31	-0.001	18993.33	0.009						
30.5	31.5	18984.18	-0.006	18993.18	-0.006						
31.5	32.5	18984.05	-0.004	18993.03	-0.016						
32.5	33.5	18983.92	-0.005								
33.5	34.5			18992.77	0.006						
34.5	35.5										
35.5	36.5										
36.5	37.5										
37.5	38.5										
38.5	39.5	18983.10	-0.013								
39.5	40.5	18982.97	0.002								
40.5	41.5	18982.83	0.006								
41.5	42.5	18982.68	-0.005								
42.5	43.5	18982.54	0.002								
43.5	44.5	18982.40	0.008								
44.5	45.5	18982.25	0.001								
45.5	46.5	18982.09	0.000								

Table 2: Molecular parameters of $^{13}\text{C}_6\text{H}$ for ground and excited $^2\Pi$ state derived from a line fit (FIT-I) and a combination difference fit (FIT-II), compared with values available from for $^{12}\text{C}_6\text{H}$ [2, 10]. All parameters are in cm^{-1} .

	$^{13}\text{C}_6\text{H}$		$^{12}\text{C}_6\text{H}$
	FIT-I	FIT-II	
B''	0.042973(16)	0.042942(17)	0.04640497
D''^a	1.20×10^{-9}	1.20×10^{-9}	1.35×10^{-9}
A''	-11.62(13)	-12.9(12)	-15.0424
B'	0.042218(17)	0.042199(17)	0.0455952(5)
D'^a	1.20×10^{-9}	1.20×10^{-9}	$1.58(28) \times 10^{-9}$
A'	-20.78(13)	-26(4)	-23.6924(7)
B'/B''^b	0.9824	n/a	0.9825
$ A' - A'' $	9.16	n/a	8.65
T_0^c	18992.116(1)	n/a	18989.7672(4)

^a Parameters fixed in the least-squares fit for $^{13}\text{C}_6\text{H}$.

^b Ratio of rotational constants is dimensionless.

^c Values in parentheses indicate the statistical error from the least-squares fit. The absolute uncertainty in T_0 is limited by the uncertainty in the frequency calibration of the laser, corresponding to 0.02 cm^{-1} .

origin (T_0), rotational parameters B'' and B' , and spin-orbit constants A'' and A' as floating parameters. We note that the centrifugal distortion constants (D'' and D') cannot be well determined with our data set, and therefore, their values are fixed to $1.2 \times 10^{-9} \text{ cm}^{-1}$. This is obtained by scaling the D'' value for $^{12}\text{C}_6\text{H}$ with the reduced mass ratio ($^{12}\text{C}_6\text{H}/^{13}\text{C}_6\text{H}$) which is derived from the rotational constant ratio. It turns out to be possible to fit both spin-orbit components simultaneously with one set of molecular parameters, yielding an overall standard deviation of 0.007 cm^{-1} , i.e., well below the experimental accuracy. The resulting constants are listed under FIT-I in Table 2. The corresponding observed-calculated (o-c) values for individual rotational transitions are also listed in Table 1. These values exhibit a statistical behavior, indicating that the spectrum is largely free of perturbations.

As no MW data for the ground state exists, it is wise to check for possible correlations between the resulting ground and upper state parameters using a global fit. Indeed, the fitted values for A and B give high correlation coefficients (1.000 and 0.997, respectively). For this, combination differences for both ground and excited state have been fitted separately. The resulting molecular parameters are summarized as FIT-II in Table 2. As can be seen, the derived values for (B'' , A'') and (B' , A') are in good agreement with those derived from FIT-I.

A simulated spectrum using these constants is incorporated in the lower panel of Figure 1. The overall pattern reproduces

well for a rotational temperature of $T_{\text{rot}} = 20.3(1) \text{ K}$. This not only applies to the Boltzmann contour, but also to the relative intensity ratio of the two spin-orbit components, indicating that the spin-orbit relaxation is as effective as the rotational cooling.

The fitted band origin of the $B^2\Pi - X^2\Pi$ band of $^{13}\text{C}_6\text{H}$ is roughly 2.35 cm^{-1} blue shifted with respect to the main isotopologue. The rotational constant $B''(^{13}\text{C}_6\text{H})$ is found to be 7.4% smaller than that of $B''(^{12}\text{C}_6\text{H})$, fully consistent with predictions from the previously determined C_6H structure in Ref. [13]. Upon electronic excitation, the value of B' decreases, indicating that the molecule stretches, but as the interatomic forces are expected to barely change, the B'/B'' ratios for $^{12/13}\text{C}_6\text{H}$ are nearly the same. It should be noted that the effective spin-orbit splitting constants ($|A''|$ and $|A'|$) for $^{13}\text{C}_6\text{H}$ are smaller than those for $^{12}\text{C}_6\text{H}$. This may be due to a different Renner-Teller effect (i.e., the electronic orbital-vibration interaction) in $^{13}\text{C}_6\text{H}$. Indeed, spin-orbit coupling can be significantly affected by Renner-Teller effects and as discussed in Ref. [10], for $^{12}\text{C}_6\text{H}$ a very strong Renner-Teller effect exists.

Acknowledgements

This work has been supported by the Netherlands Foundation for Fundamental Research on Matter (FOM) and the Netherlands Organisation for Scientific Research (NWO) through a VICI grant and within the context of the Dutch Astrochemistry Network (DAN). X.B. and W.U. acknowledge support from the Templeton Foundation.

References

- [1] J.C. Pearson, C.A. Gottlieb, D.R. Woodward, P. Thaddeus, *Astron. Astrophys.* 189 (1988) L13–L15.
- [2] H. Linnartz, T. Motylewski, O. Vaizert, J.P. Maier, A.J. Apponi, M.C. McCarthy, C.A. Gottlieb, P. Thaddeus, *J. Mol. Spectrosc.* 197 (1999) 1–11.
- [3] C.A. Gottlieb, M.C. McCarthy, P. Thaddeus, *Astrophys. J. Suppl. S.* 189 (2010) 261–269.
- [4] H. Suzuki, M. Ohishi, N. Kaifu, S. Ishikaw, T. Kasuga, *Publ. Astron. Soc. Jpn.* 38 (1986) 911–917.
- [5] J. Cernicharo, M. Guelin, K.M. Menten, C.M. Walmsley, *Astron. Astrophys.* 181 (1987) L1–L4.
- [6] J. Cernicharo, M. Guelin, C. Kahane, *Astron. Astrophys. Suppl. S.* 142 (2000) 181–215.
- [7] P. Freivogel, J. Fulara, M. Jakobi, D. Forney, J. P. Maier, *J. Chem. Phys.* 103 (1995) 54–59.
- [8] M. Kotterer, J.P. Maier, *Chem. Phys. Lett.* 266 (1997) 342–346.
- [9] T. Motylewski, H. Linnartz, *Rev. Sci. Instrum.* 70 (1999) 1305–1312.
- [10] D. Zhao, M.A. Haddad, H. Linnartz, W. Ubachs, *J. Chem. Phys.* 135 (2011) A044307.
- [11] D. Zhao, N. Wehres, H. Linnartz, W. Ubachs, *Chem. Phys. Lett.* 501 (2011) 232–237.
- [12] PGOPHER, a Program for Simulating Rotational Structure, C.M. Western, University of Bristol, <http://pgopher.chm.bris.ac.uk>.
- [13] M.C. McCarthy, P. Thaddeus, *J. Chem. Phys.* 122 (2005) 174308.